JTTEE5 13:544-553
DOI: 10.1361/10599630419382
1059-9630/$19.00 © ASM International

Peer Reviewed

Columnar Grain Growth of Yttria-Stabilized-Zirconia in Inductively Coupled Plasma Spraying

In Ha Jung, Ki Kwang Bae, Kee Chan Song, Myung Seung Yang, and Son Ki Ihm

(Received January 13, 2003; in revised form May 22, 2003)

Yttria-stabilized-zirconia (YSZ) was deposited 7 mm thick by inductively coupled plasma spraying (ICP) and a theory of nucleation and solidification of YSZ was introduced. The concentration was homogeneous within a particle, but different from particle to particle. The solute rejection by diffusion occurred in a layer during solidification, but the interface condition of $(dT_q/dz)_{z=0} > m(dC/dz)_{z=0}$ led columnar grains to facilitate. The microstructure of the bottom part showed small equiaxed grains. In the middle part, large columnar grains, about 100 μm thick and 300 μm long, were developed through the layers with strong adhesion. Heat of droplets, latent heat of solidification, small pore array in the splat boundaries, and low thermal conductivity retard the heat transfer, and thus thick and long columnar grains could be facilitated. The long columnar grain growth through the layers was supposed to be possible when the previously solidified surface of the deposit acts as seed.

Keywords columnar grain, microstructure, plasma spray, thick deposit

1. Introduction

Many rapid solidification processes (RSPs) have been developed in the past, such as splat quenching, melt spinning, planar flow casting, laser or electron beam resolidification, atomization, bulk undercooling, and so forth (Ref 1, 2). These processes can be classified into three main groups—laser surface treatment/welding, planar flow casting/melt spinning, and bulk undercooling/atomization—which show distinct and important differences in processing parameters. Thermal spray deposition has been grouped in planar flow casting/melt-spinning process (Ref 2, 3).

In a thermal plasma spraying system, particles are melted independently of each other and fall on the substrate or previously deposited layer and subsequent solidification occurs. Wang et al (Ref 3). developed an integrated model to predict the microstructure formed by a thermal plasma spray. To illustrate the applicability of the model, the rapid solidification of 5 μm thick Al- 5wt.%Cu melt was simulated under various interfacial heat transfer and undercooling conditions. The 5 μm thick splats built on copper substrate showed the temperature gradient 10^4 to 10^6 K/m and interface velocity near 200 m/s. This would belong to rapid solidification condition, so melt-spinning model should be applied (Ref 3-6).

On the other hand, for thick deposits with zirconia stabilized with 20 wt.% yttria (YSZ) powder on a graphite substrate by an inductively coupled plasma (ICP) spraying system, the temperature of the droplets is so high as to evaporate the skin of particles. In addition, the plasma flame heats the substrate or deposit during solidification (Ref 7). Moreover, the lower heat conductivity of YSZ (4 W/m s) than that of metals retards heat transfer. In this condition, the rate of interface movement is so slow that a steady-state condition can be applied. Most of the solidification processes of single crystal for optical and electronic compound semiconductors, such as GaAs, InP, and InGaAs, belong to this category. The temperature gradient is in the range of 40 to 60 °C/cm and the rate of interface movement is 0.6 to 2.0 mm/h (Ref 8).

According to Kurz (Ref 5), a cellular or planar surface can be developed either the lower rate of interface movement below 10^{-4} mm/s or the higher rate of more than 10 mm/s. YSZ solidification processes in the plasma spraying system may belong to the first category, while the results observed by Wang et al. (Ref 2) are supposed to be the latter.

Microstructures such as equiaxed, columnar, or dendrite depend on the rate of interface movement, temperature gradient, solute and thermal diffusion rate, concentration of solute, and so on.

In this article, a theory related to nucleation and solidification of YSZ in ICP is introduced, and the microstructure of YSZ deposit of more than 7 mm thick is taken into account. It was interpreted by lower rate of interface movement range, below 10^{-4}mm/s (Ref 5). The subjects described with equations are undercooling (ΔT), nucleation, grain growth, and its thermodynamics, solute rejection, and thermodynamic effects on the rate of interface movement. A microstructure of the YSZ deposit, stability criteria of the interface, and continuous grain growth phenomena in ICP spraying system are also described.

In Ha Jung, Department of Chemical Engineering, Korea Advanced Institute of Science and Technology, 373-1 Kuson-dong, Yusong-gu, Taejon, Korea, 305-701 and Department of DUPIC Nuclear Fuel Development, Korea Atomic Energy Research Institute, P.O.Box 105, Yusong, Taejon, Korea, 305-353; **Ki Kwang Bae, Kee Chan Song,** and **Myung Seung Yang,** Department of DUPIC Nuclear Fuel Development, Korea Atomic Energy Research Institute P.O.Box 105, Yusong, Taejon, Korea, 305-353; and **Son Ki Ihm,** Department of Chemical Engineering, Korea Advanced Institute of Science and Technology, 373-1 Kuson-dong, Yusong-gu, Taejon, Korea, 305-701. Contact e-mail: nihjung@nanum.kaeri.re.kr.

2. Solidification Theory (Ref 4-6, 9-11)

2.1 Undercooling

2.1.1 Thermal Undercooling. Thermal undercooling ΔT_t is related to the imposed temperature gradient by heat extraction out from the system, and it is usually defined as the temperature difference between the equilibrium temperature of a system and its actual temperature.

Heat extraction changes the energy of the phases (solid and liquid) in two ways, a decrease in the enthalpy of the liquid or solid ΔH and the latent heat of fusion due to the transformation from liquid to solid ΔH_f. The resultant cooling rate dT/dt, can be deduced as Eq 1 from a simple heat balance if the material is isothermal (low cooling rate) and the specific heats of the liquid and the solid are the same:

$$\frac{dT}{dT} = \dot{T} = \frac{-q_e\left(\frac{A'}{v\,c}\right)}{1-\left(\frac{\Delta h_f}{c}\right)\left(\frac{df_s}{dT}\right)} \qquad \text{(Eq 1)}$$

where q_e is the external heat flux, A' and v are the surface area and the volume of the deposit, c and Δh_f are the specific heat and the latent heat per unit volume, and f_s is the fraction of solid.

The magnitude of undercooling can be described with above heat balance and a lever rule (Ref 12). Suppose that the powder of composition C_0 is melted in plasma and locally cooled on the substrate to T^*, which is slightly below its melting point. At the liquid/solid interface, the concentrations of liquid and solid in local equilibrium will be C_l^* and $C_l^* k$ with volume fractions of a and b, respectively, where k is a distribution coefficient defined as a solute ratio of solid to liquid in an alloy, determined by their solubilities.

The magnitude of local thermal undercooling (ΔT_t) of the solid in small volume at equilibrium can be defined as:

$$\Delta T_t = \Omega\,\frac{\Delta h_f}{c} \qquad \text{(Eq 2)}$$

where Ω is the solutal supersaturation $b/(a+b)$ by definition (Ref 12).

2.1.2 Solute undercooling (ΔT_c) is related to the solubility of the solute in an alloy. In an alloy, as the interface advances, solute will be rejected if the solubility of the solute in solid is lower than that in the liquid. When the interface has been advancing for some time, the concentration distribution becomes time-independent (steady-state). Under this condition, the concentration in the liquid C_l decreases exponentially from the maximum composition C_0/k at the interface to the original composition C_0 far from the interface, as shown in Fig. 1 (Ref 13). However, the liquid temperature T_l (the melting point) of the alloy will increase as z increases, indicated on the right and left lower

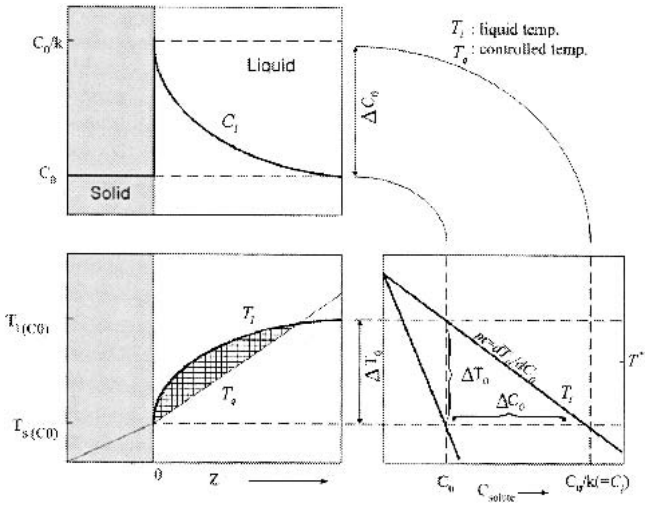

Fig. 1 Solute undercooling in alloy

Table of Symbols

A	surface area of a nucleus
A'	surface area of a deposit
C_0	initial alloy concentration
C_l	concentration of liquid
C^*	concentration at solid/liquid interface
D	diffusion coefficient in liquid
I	nucleation
K	curvature
T_f	melting point
$T_{l(C0)}$, $T_{s(C0)}$	liquid and solid temperatures corresponding to the initial alloy composition C_0
T_l	temperature of liquid
T^*	temperature of solid/liquid interface
T_q	temperature imposed by the external heat flux
V	rate of interface movement
a, b	volume fractions of liquid and solid
c	specific heat per unit volume
f_s	fraction of solid
k	distribution coefficient
m	slop of the liquidus line
q_e	external heat flux
r^0	critical radius of a cluster
z	distance from solid/liquid interface
ΔG	Gibbs free energy change
ΔG_n^0	maximum activation energy for nucleation of a critical number of n clustered atoms
ΔG_d	activation energy for diffusion across solid/liquid interface
Δg	Gibbs free energy change per unit volume
ΔH	enthalpy
ΔH_f	latent heat of fusion
Δh_f	latent heat per unit volume
Δs_f	entropy of fusion per unit volume
ΔT_c	solute undercooling
ΔT_r	curvature undercooling
ΔT_t	thermal undercooling
Γ	Gibbs-Thomson coefficient
Ω	solutal supersaturation
θ	wetting angle
v	volume of a deposit
σ	solid/liquid interface energy

side in the figure. This means that if small volumes of the liquid at various distances ahead of the interface were extracted and solidified, their equilibrium solidification points would vary with positions. Each volume element finds itself at a temperature, T_q, which is an imposed temperature gradient caused by a heat extraction. At the solid/liquid interface ($z = 0$) if T_q is less than T_l, there exists a volume of liquid that is undercooled and in a higher Gibbs free energy state than that of solid. This (cross-hatched) region is called a zone of constitutional or solute undercooling and has a potential for development of a dendrite in an alloy.

2.1.3 Curvature undercooling (ΔT_r) is related to a tip size of the grain. Consider the small cluster or nucleus of radius r in a liquid. Surface tension will tend to contract the surface area and the internal volume, increasing the internal pressure by an increment ΔP. This occurs because the small radius of curvature creates a pressure difference between the cluster and the liquid in the surroundings. The equilibrium melting point is thus lowered by an amount of ΔT_r. It is inversely proportional to a radius of a crystal, as shown in Eq 3 (Ref 14):

$$\Delta T_r = \frac{2\Gamma}{r} = K\Gamma \qquad \text{(Eq 3)}$$

where K is a curvature and is equal to the ratio of surface area change to the change of the volume (dA/dn) of the nucleus. Γ is the Gibbs-Thomson coefficient (= $\sigma/\Delta s_f$, σ is the solid/liquid interface energy, J/m^2; Δs_f is entropy of fusion per unit volume, J/m^{3}K).

2.2 Nucleation, Growth, and Its Thermodynamics

At the beginning of solidification, small clusters of atoms appear in the liquid. This is called a cluster or embryo, and smaller size than its critical size of r^0, which is the allowed size at equilibrium. The Gibbs free energy change for nucleation of 1 mol in liquid is the sum of the interface energy term and volume term (Ref 15).

$$\Delta G = \Delta G_i + \Delta G_v = \sigma A + \Delta g \cdot v \qquad \text{(Eq 4)}$$

Assuming a spherical form of nucleus with minimum surface area, Eq 4 will be:

$$\Delta G = \sigma 4\pi r^2 + \frac{\Delta g\ 4\pi r^3}{3} \qquad \text{(Eq 5)}$$

where Δg is the Gibbs free energy change from liquid to solid per unit volume, which becomes $-\Delta s_f\, \Delta T$ at constant pressure. ΔT, undercooling, is a difference between melting point (T_f) of material and its real liquid temperature (T) at the interface. The maximum size of r^0 of crystal nucleus can be obtained from the first derivative of Eq 5 set to zero and rearranged by r^0, that is:

$$r^0 = -\frac{2\sigma}{\Delta g}, \quad \text{at} \quad \frac{d(\Delta G)}{dr} = 0 \qquad \text{(Eq 6)}$$

This result is equal to that from Eq 3 of the curvature undercooling, since $\Delta g = -\Delta s_f\, \Delta T$ and $\sigma = \Gamma \Delta s_f$.

The maximum value of activation energy for nucleation of a critical number of n clustered atoms ΔG_n^0 can be obtained by substituting $r = -2\sigma/\Delta g$ into Eq 5; therefore:

$$\Delta G_n^0 = -\left(\frac{16\pi}{3}\right)\left(\frac{\sigma^3}{\Delta g^2}\right)\Bigg|_{r=r^0} = -\frac{16\pi}{3}\cdot\frac{\sigma^3}{(-\Delta s_f \cdot \Delta T)^2} \qquad \text{(Eq 7)}$$

The clusters that overcome this activation energy will grow larger than r^0 in the liquid, and become large grains.

Besides the nucleation energy ΔG_n^0, forming clusters will require the transfer of atoms from the liquid to nuclei. Activation energy ΔG_d for transfer through the solid/liquid interface must therefore be considered. In steady state, the nucleation rate in liquid per unit volume and time I is given by (Ref 16):

$$I = I_0 \exp\left(-\frac{\Delta G_n^0 + \Delta G_d}{k_B T}\right) \qquad \text{(Eq 8)}$$

Where I_0 is a pre-exponential factor. This equation contains two exponential terms. One is ΔG_n^0, varies as $-1/T\Delta T^2$ (Eq 7), while the other, ΔG_d, varies as $-1/T$. An increase in ΔT, giving more numerous and smaller nuclei, is accompanied by a decrease in T, but fewer atoms are transferred from the liquid to nuclei.

According to the cooling rate, liquid drop may be either a glass or a crystal. When liquid drops are cooled, the cooling curve will generally cross the nucleation curve in the TTT diagram. However, the very high rate of heat removal can cause the cooling curve to miss the nucleation curve completely and an amorphous solid is then formed. This microstructure can be easily seen in air plasma spraying (APS) or vacuum plasma spraying (VPS) systems (Ref 17-24). The cooling rate of this process is very rapid and has to be interpreted by rapid solidification theory as done by Wang et al. (Ref 2).

2.3 Solute Rejection at the Solid/Liquid Interface and Its Effect on the Microstructure

The undercooled region, which is described in Section 2.1 and Fig. 1, will affect the local equilibrium solidification temperature T_l of the liquid, which is related to the composition by (Ref 25):

$$T_{l(C0)} - T_{s(C0)} = m(C_0 - C_l) \qquad \text{(Eq 9)}$$

where $T_{l(C0)}$ and $T_{s(C0)}$ are liquid and solid temperatures corresponding to the initial alloy composition C_0, m is the slope of the liquidus line, and C_l is the solute concentration of the liquid that is equal to C_0/k. This relationship is shown in Fig. 1. It indicates that the concentration boundary layer can be converted, by using the phase diagram, into a liquidus temperature boundary layer. The liquid temperature increases with increasing z, when the value of k is less than unity and in the case of the negative slope of m. To investigate the stability of the solidifying surface, it is also necessary to determine the temperature T_q imposed by the external heat flux and its temperature gradient $(dT_q/dz)_{z=0}$ at the interface.

At the solid/liquid interface, depending on the temperature gradient, there may, or may not, exist a zone of constitutional undercooling. The condition required for a constitutionally undercooled zone is that the temperature gradient is lower than the gradient of liquidus temperature $(dT_l/dz)_{z=0}$ at the interface. The

latter gradient is obtained by multiplying the concentration gradient, $(dC/dz)_{z=0}$, by the liquidus slope, m. Therefore, the interface is constitutionally undercooled when:

$$\left(\frac{dT_q}{dz}\right)_{z=0} < m \cdot \left(\frac{dC}{dz}\right)_{z=0} \quad \text{(Eq 10)}$$

when the right hand side of Eq 10 is smaller than the temperature gradient, planar surface or columnar grain growth is favorable at the solid/liquid interface (Ref 26).

3. Experimental Procedure

Zirconia stabilized with 20 wt.% yttria (AMDRY146, fused and crushed, cubic, T_m = 2970 K, METCO Westbury, NY) powder was used as feedstock. Table 1 shows the chemical compositions in weight percent of yttrium and zirconium analyzed by inductively coupled plasma-atomic emission spectrometer (ICP-AES; model JY50P, Jobin Yvon, France). The feedstock was noted by −45, −75, and −90 μm. In this article, a description of −45 μm means the powder was sieved with ASTM No. 325, −75 μm with ASTM No. 200, and −90 μm with ASTM No. 170. The average diameters of each powder are shown in Table 1. The particle size was measured by a particle size analyzer (MAE5000, Malvern, UK).

ICP spraying equipment (100 kW, 300kHz), a cylindrical spraying chamber, diameter 1.1 m × length 1.8 m with double walls and a water-cooling system was used. The detail schematic drawing of the powder deposition equipment was shown in previous paper (Ref 7). A volumetric powder feeder (CYLCO, Sylvester company, OH) with an 8 threads/in. driving screw was used. Ar gas was supplied as the powder carrier gas, and the powder hopper was vibrated to feed the powder smoothly. Ar gas was also used as the central gas, and H_2 with Ar was used as the sheath gas. Experimental conditions are summarized in Table 2.

Table 1 Chemical composition and average particle sizes of the feedstock

Chemical composition, wt.%			Particle size, μm		
Y	Zr	O	−45	−75	−90
16.6	55.4	28	28	31.8	39

Table 2 Summary of YSZ powder deposition conditions

Parameters	Condition
Central gas flow rate, Ar, L/min	35
Powder feed rate, g/min	16.6
Carrier gas flow rate, Ar, L/min	5
Chamber pressure, torr	200
Powder spraying distance, Z_s, cm	22
Sheath gas composition, G_{comp}, L/min	120(Ar)/20(H_2)
Probe position, Z_p, cm	8
Particle size, μm	−90, −75, and −45

After evacuating the chamber to 50 torr (0.067 bar), the plasma was ignited, and then the chamber pressure was adjusted to 200 torr (0.267 bar). To observe the degree of particle melting during spraying, a water bath of 280 mm diameter was laid on the bottom of the chamber, or closely positioned to the spray nozzle for observing the particle morphologies after rapid quenching.

To fabricate the deposits, a rectangular graphite bar, 25 by 25 by 40 mm, was used as a substrate. For a thick deposit, about 7 mm thick, powder was sprayed for about 20 to 60 s. The specimens were cooled in Ar atmosphere for 30 min. The specimens were then separated from the substrate and cut vertically by a diamond saw (Isomet 2000, Buehler). A cut section of the deposit was etched with a 50% hydrogen fluoride solution heated to its boiling point.

To obtain the samples of splats, powder was sprayed for a short time on a 2 mm thick stainless steel plate fixed on a graphite substrate.

A scanning electron microscope (SEM; Jeol JSM 840A, Japan Electron Optics Ltd., Tokyo, Japan) and an optical microscope (Letiz METALLUX 3, IA) were used to study the microstructure of the deposit. Chemical composition of the spheroidized particles and deposits were measured by electron probe microscope analyzer (EPMA) (model SXR, CAMECA, Paris, France) with a beam size of 1 μm. The phases were analyzed by x-ray diffraction (XRD) (MXP3A-HF, Mac Science, Ishikawa, Japan) using Cu $K\alpha_1$ radiation with a graphite monochromator. The scanning angle was between 20° and 100° at the interval of 0.05° using a step counting time of 3 s. A transmission electron microscope (TEM) (JEOL 2000 FX2, JEOL, MA) was used to observe internal microstructure. Samples were prepared by mechanical thinning, followed by ion milling.

4. Results and Discussion

4.1 Yttrium Concentration Profile of Spheroidized Particles

The concentration of Y of a spheroidized particle in radial direction within the particle were no different, regardless of either particle sizes or spraying conditions. It was measured by EPMA of 1 μm probe size every 2 μm, although the results are

Table 3 Average diameter of the feedstock and spheroidized particle

Classification	Diameter of feedstock, μm	Diameter of spheroidized particle, μm	Splat thickness, μm	Splat diameter, μm	Degree of deformation(a), %
−45 μm	28	31	1.97	100	323
−75 μm	31.8	34	2.14	110	324
−90 μm	39	41	2.7	130	317

Spraying condition: Ar/H_2 = 120/20 L/min, chamber pressure 200 torr, Z_p = 8 cm and Z_s = 22 cm. (a) Degree of deformation, % = Splat diameter/Spheroidized particle diameter × 100

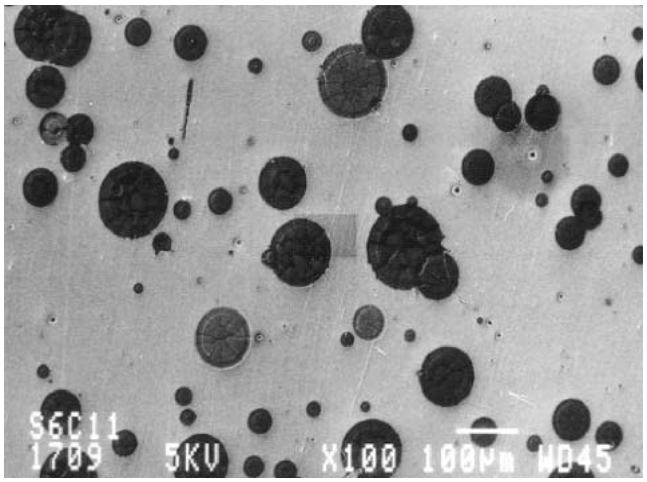

Fig. 2 Microstructure of the splats (spraying condition: particle size, −75 μm; Ar/H_2 = 120/20 L/min; chamber pressure, 200 torr; Z_p = 8 cm; Z_s = 22 cm)

not shown here. The average Y concentration was 16.70 wt.% with standard deviation of 0.5 wt.%. This illustrates that zirconia (T_m = 2970 K) and yttria (T_m = 2700 K), although their melting points are not the same, were melted without separation or selective evaporation during spraying. That is, almost all the particles were solid solution during melting. Much evaporated submicron particles were observed on the spraying chamber wall after several runs of experiments. On the other hand, the concentration was different from particle to particle by standard deviation of 4.82 wt.% in Y. In sampled particles, the lowest Y concentration was 6.28 wt.%, and the highest was 21.07 wt.%. This may come from the manufacturing process of the powder. The result of average concentration of the spheroidized particles was in good agreement with that of the feed powder.

4.2 Diameter and Thickness of Splat

Table 3 represents the average diameters of the spheroidized particles of three different particle sizes of −45, −75, and −90 μm. The thickness of the splat in Table 3 was directly measured in SEM image from the cut section of the deposit about 7 mm thick. It showed 2 to 3 μm, depending on the particle sizes. Then, the average splat diameters were calculated from the observations of spheroidized particle diameter and splat thickness, and obtained as 100 to 130 μm. There exists about 5% difference between calculated and observed data. The degree of deformation of the splat over the diameter of the spheroidized particle was approximately 320%. This is larger than the other experiment results (Ref 27), which illustrates that the dwell time of particles in ICP is longer than in APS or VPS. Figure 2 shows the sample of splats. The splats are shown many small grains in their inner part.

4.3 X-ray Diffraction Analysis

For XRD analysis of a deposit, the modeling condition by Scardi (Ref 28) was based on the relative concentration of yttria as 13.2 mol.% (16.49 wt.% Y), the same as the result of EPMA quantitative analysis of spheroidized particles. Quality factors of the fitting, R_{wp} = 9.92 and χ^2 = 5.28, showed the high reliability of the refinement. It showed that about 3% of the tetragonal phase of a lattice parameters with a = 3.614(1) Å and c = 5.124(4) Å was contained in cubic matrix with a = 5.1430(2) Å. The existence of a small tetragonal phase agrees with the result of EPMA analysis on the spheroidized particle described in Section 4.1 because the tetragonal phase is stable at low Y contents. Figure 3 shows a TEM micrograph of the tetragonal phase and its index. Low Y content results in a tetragonal phase. The t-ZrO_2 is identified by the weak (211) superlattice-type reflections. Reflections of the type (100) and (110) disappear for the t-ZrO_2 but appear by multiple diffraction (Ref 29).

The boundary of the columnar grain and the splat can be clearly observed in TEM as shown in Fig. 3 and its small window, at which an array of small pores can be seen. These pores may be the trapped gas from the plasma gas during spraying. If they originated from the interior of the particle itself and subsequently moved along the solidification interface, they must be observed in the interior of the splats as well. Therefore, most pores in the particle were supposed to be pulled out during melting and falling down. This array of pores at the boundary of the splats may retard the heat transfer.

4.4 Microstructure of the Deposit and Solidification Mode

The microstructure about 7 mm thick deposited by ICP had a lamellar and columnar structure perpendicular to the spraying direction. In the bottom part near the substrate, equiaxed and columnar grains bound in a layer, a “brick wall” (named by Sampath and Herman Ref 30), pores, and cracks were observed. In the middle part, relatively regular sized columnar grains, about 100 μm thick and 300 μm long, through many layers with excellent bonding and dense microstructure, were distinguished. In the upper part, the microstructure was the same as the middle, but the sizes of columnar grains were irregular.

The shape of the layer depends on the ability to adhere by impact and deformation on the substrate or previously solidified splats (Ref 20, 31, 32). However, the bottom layers close to the graphite substrate were generally fine and equiaxed grains. Partly, they were columnar grains separated by a horizontal gap due to poor contact between layers and vertical crack, as shown in Fig. 4. A fine-grained equiaxed microstructure was normally observed in APS or VPS spraying systems (Ref 18, 21-23). In APS or VPS system, the dwell time of particles is not so long compared with the ICP that full melting of particle is difficult (Ref 33). Moreover, the characteristic of short plasma flame makes the substrate remain at low temperature. An increase in temperature difference between the droplet and the substrate results in more nuclei of the fine grains (Ref 24). In this experiment, the bottom layer was deposited at first on a cold substrate before heating by the droplets or plasma flame. According to Eq. 6 to 8, a large ΔT gives rise to more numerous and much smaller grains. Therefore, smaller equiaxed grains are likely to be seen on the cold substrate at the beginning of spraying. The grains solidificated on the graphite substrate were small equiaxed grains of 0.5 to 1 μm. According to the Eq 3, the amount of curvature undercooling for an equiaxed grain of 0.5

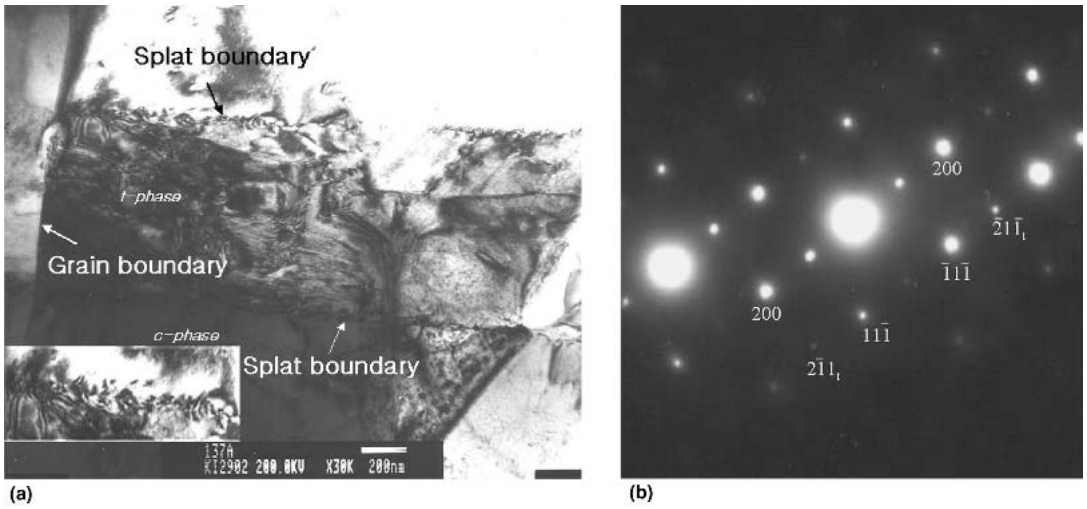

Fig. 3 (a) Microstructure of the columnar grain through the layers. (b) Diffraction pattern of t-phase (deposition condition: particle size, −75 μm; Ar/H_2 = 120/20 L/min; chamber pressure, 200 torr; Z_p = 8 cm; Z_s = 22 cm)

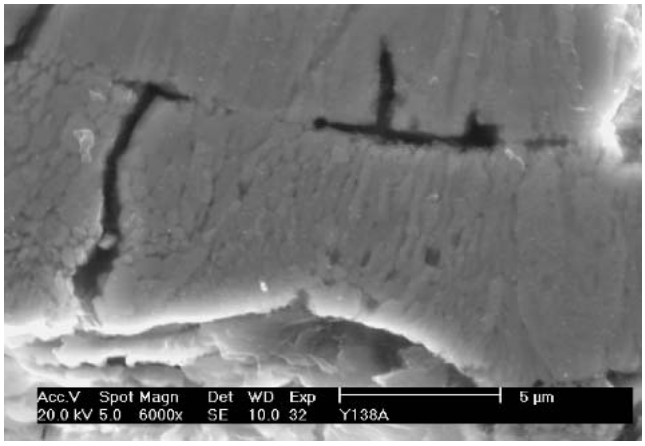

Fig. 4 Microstructure of YSZ splats solidificated on the surface of the graphite substrate (deposition condition: particle size, −75 μm; Ar/H_2 = 120/20 L/min; chamber pressure, 200 torr; Z_p = 8 cm; Z_s = 22 cm)

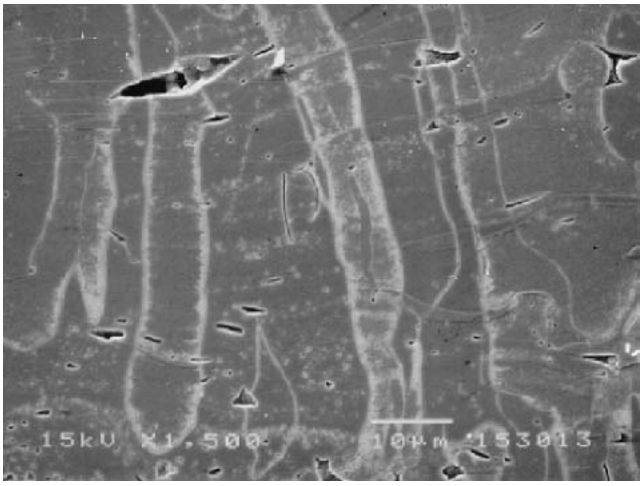

Fig. 5 Columnar grains developed in the middle part of the deposit (deposition condition: particle, size −75 μm; Ar/H_2 = 120/20 L/min; chamber pressure, 200 torr; Z_p = 8 cm, Z_s = 22 cm)

μm estimated by 52 K, when σ = 1 N/m and Δs_f = 79,142 J/m^2 · K (Ref 34).

In the middle part of the deposit, no boundary lines between layers were observed. The grains were grown through the layers. Figure 5 shows the long columnar grains developed in the middle part of the deposit and Fig. 6 shows its fractured surface. Grains were thicker and longer than the other parts, and some of the grains reached 100 μm thick and 300 μm long. According to the Eq 1, it is seen that the solidification rate of the deposit decreases gradually since df_s/dT is negative, and the term of A'/v is decreased as increasing the height of the deposit. The magnitude of local thermal undercooling ΔT_t, estimated by 2.6K when Ω = 1/10, Δh_f = 36,729 J/kg[34] and c = 1407 J/kg · K[35] by Eq 2. The solutal supersaturation Ω was calculated from the phase diagram (Ref 36).[36] This small thermal undercooling may be due to the heat of droplets, latent heat of solidification (recalescence effect), small pore array in the splat boundary as well as the low thermal conductivity of the YSZ, resulting in retarding the heat removal and decreasing the solidification rate. During spraying, the temperature of the substrate was reached by 2100 K.[37]

Following Kurz (Ref 24), at high and even temperature of the deposit and low solidification rate, the solid/liquid interface grows as planar. Sampath et al. (Ref 18) observed a columnar grain with zirconia 8 wt.% yttria, but the grain size was limited to a layer boundary. The other works have observed similar size of small grains (Ref 38-42); this may be due to the low substrate or deposit temperature of the APS process and rapid solidification without grain growth.

When a new droplet starts to solidify, liquid phase on the splat may enforce the bonding. The source may be the remaining liquid in the previously deposited layer surface, or remelt by the heat of the new droplet. A fractured surface showed a perfect bonding structure between the splats, which was shown in Ref 7. Somewhat different colors among the layers allude to different

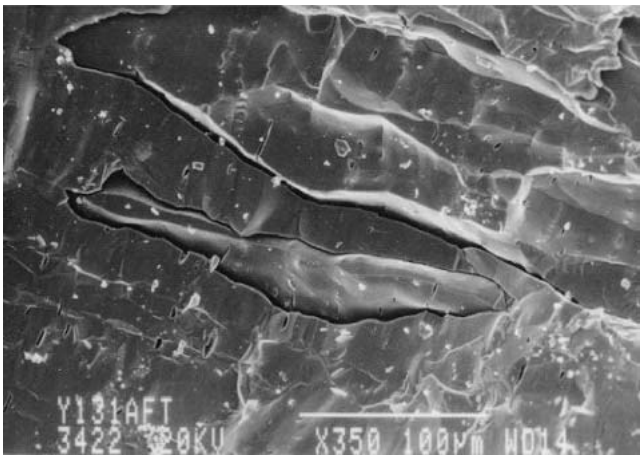

Fig. 6 Microstructure of columnar grains in a fractured surface (deposition condition: particle size, −75 µm; Ar/H_2 = 120/20 L/min; chamber pressure, 200 torr; Z_p = 8 cm; Z_s = 22 cm)

solidification conditions. Strong adhesion between the splats may result from the physical and metallurgical interaction mechanisms (Ref 21).

4.5 Yttrium Concentration Profile of the Layers in the Deposit

Figure 7 shows a middle part of a deposit sprayed at the condition of particle size −75 µm, Ar/H_2 = 120/20 l/min, chamber pressure 200 torr, Z_p = 8 cm, and Z_s = 22 cm. The substrate is positioned on the left of the figure. The Y concentration profile is marked on the figure for distance of 43 µm with 120 points. The average concentration of Y along the measured length represented 14.47 wt.%, and the standard deviation was 4.64 wt.%. The discrepancy with the average concentration of spheroidized particles of 16.49 wt.% is due to the contained lower Y concentration layers of 4 to 7 wt.%. This may be caused by the uneven concentration of each feed particle. However, the concentration gradient of the interlayer boundaries was linear in the range of 0.5 to 1 µm, although each particle has a discrete concentration. This infers that atoms diffuse each other between the layers. Figure 7 also shows the concentration fluctuation of Y in each layer. This may come from different solidification conditions such as particle size and their heated temperature, spraying time gap between layers, and cooling rate, and so forth.

Section 2 explains that solid/liquid interface rejects solute into the liquid, when m is negative and k is less than unity. According to Kurz (Ref 43), assuming the existence of local equilibrium, directional solidification with a planar solid/liquid interface can divide into three transient states, that is, initial transient, steady state, and final transient. When the droplet with C_o of solute concentration solidify, the solid will have the solute concentrations of $C_o \cdot k$ at initial transient, C_o at steady state, and C_o/k at final transient, as shown in Fig. 1. Therefore, the solute distribution of the solid has a similar shape with the S curve after completing the solidification, which causes so-called segregation in the alloy at final transient. However, the average solute concentration in a layer is the same as its feed particle. The yttrium concentration of a layer, marked 1 in Fig. 7, corresponds to this case.

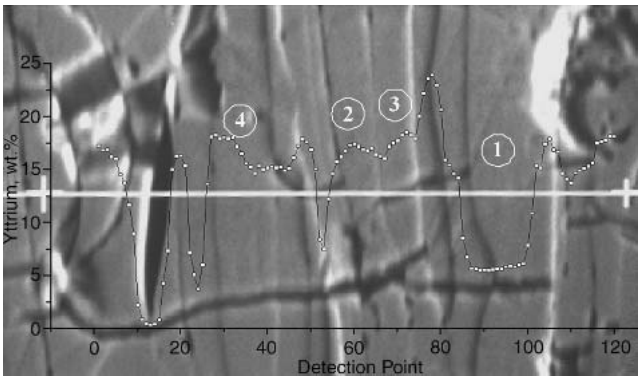

Fig. 7 Yttrium concentration profile through the layers (deposition condition: particle size, −75 µm; Ar/H_2 = 120/20 L/min; chamber pressure, 200 torr; Z_p = 8 cm; Z_s = 22 cm)

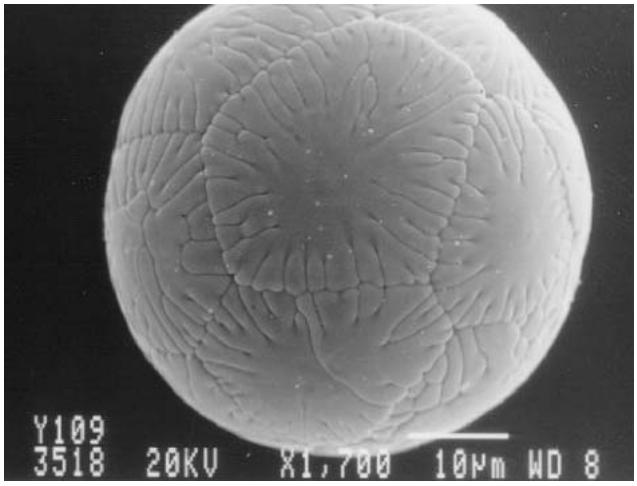

Fig. 8 Dendrite microstructure of the rapidly quenched YSZ particle in the water bath

On the other hand, assuming that the new liquid droplet comes down on the previously deposited layer, which is in the steady state among the three transient states of solidification. The solute, highly piled up in final transient, can be transported into the newly deposited layer by diffusion or by convection (or both) due to its high temperature or shock of impact. Then it proceeds from an initial transient, steady state, to the final transient, one after another. These phenomena can be seen on the layers marked 2 and 3 in Fig. 7. It shows a maximum solute content at the starting point of mixing by impact.

The layer marked 4 in Fig. 7, the solute concentration shows a reverse S curve, showing the higher yttrium content at the starting point of solidification. This can occur when the solidification rate is faster than the diffusion rate, which is called solute trapping (Ref 44). When the liquid drop comes down and wets on the previously deposited layer, which is in a somewhat cooled state, large ΔT is induced, and this leads to a solute trapping by some distance. Then, the interface turns to the state of normal solidification by heat of fusion and heat of new droplet.

However, it is important that even though the concentration of the solute fluctuated due to the solute rejection during solidi-

fication in a layer, its average value was almost the same as its droplet. Even though the solute rejection occurred during solidification, the interface condition of $(dT_q/dz)_{z=0} > m(dC/dz)_{z=0}$ led to facilitate columnar grains.

4.6 Stability Criteria of the Interface

One can derive stability criteria of the solidification interface of a deposit from the relationship between concentration and temperature profile in solid/liquid interface for preventing the undercooled region (shown in Fig. 1 as crosshatched area under the liquidus curve) so the plasma sprayed deposits exhibit columnar microstructure (Ref 45). The YSZ solidification condition of this experiment can be simplified as follows:

- unidirectional solute (yttria) diffusion at solid/liquid interface
- $k = C_s/C_l < 1$: from the YSZ phase diagram (Ref 36)
- Rate of solute rejection equals the diffusional flux in the liquid at the interface
- Grain growth in the opposite direction of heat removal
- Steady state

From Fick's second law for one-dimensional system:

$$\frac{\partial^2 C}{\partial^2 z} + \frac{V}{D}\frac{\partial C}{\partial z} = 0 \qquad \text{(Eq 11)}$$

where D is a diffusion coefficient of the solute in liquid, z is the position of solid/liquid interface, and V is the rate of interface movement, dz/dt. Equation 11 can be solved by applying the B.C., $C = C_0$ when z goes to infinity, and the rate of solute rejection equals the diffusional flux at the interface; that is, $C^*(1 - k)V = -D(dC/t)$ at $z = 0$, as assumed earlier in this section and where, C^* is the concentration of the solute at the solid/liquid interface. Therefore, the complete solution of Eq 11 for the solute distribution ahead of solid/liquid interface, advancing under steady-state conditions, is:

$$C = C_0 + \Delta C_0 \exp\left(-\frac{Vz}{D}\right) \qquad \text{(Eq 12)}$$

Differentiating Eq 12 at $z = 0$ and from the relationship between concentration and temperature gradient as shown in Eq 9 gives

$$\left(\frac{dC}{dz}\right)_{z=0} = -\frac{V}{D}\Delta C_0 \qquad \text{(Eq 13)}$$

where $\Delta T_0 = T_{l(C0)} - T_{S(C0)}$ and $\Delta C_0 = C_l - C_0 = C_0(1 - k)/k = -\Delta T_0/m$ as shown in Eq 9 and Fig. 1. Therefore, the condition for facilitating the planar or columnar surface should become:

$$\left(\frac{dT_q}{dz}\right)_{z=0} > m\left(\frac{dC}{dz}\right)_{z=0}\left[=\frac{V\Delta T_0}{D}=\frac{V}{D}\cdot\frac{mC_0(k-1)}{k}\right] \qquad \text{(Eq 14)}$$

Therefore one can summarize the stability criteria of the deposit by comparing the temperature gradients between equiaxed or dendritic and planar or columnar grain, as shown in Table 4.

Table 4 Stability criteria of solidification interface of deposit

Growth condition	
$(dT_q/dz)_{z=0} < m(dC/dz)_{z=0}$	$(dT_q/dz)_{z=0} > m(dC/dz)_{z=0}$
Unstable	Stable
Dendrite or equiaxed grain	Planar or columnar

For Zr with 20 and 10 wt.% yttria, the minimum stabilizing temperature gradient can be inferred from Eq 14 as shown in Table 5 with a function of a distribution coefficient. The substituted values were: $D = 0.005$ mm^2/s, $V = 10^{-4}$ mm/s (Ref 46), and slope of liquidus line from phase diagram of YSZ, $m = -0.64$ K/wt%. The minimum stabilizing temperature gradient of YSZ was evaluated to 1/100 to 1/1000 times of Al-5wt.%Cu system (Ref 2). This may be from the difference of the slope of liquidus line in the phase diagram between two materials and the solidification rate assumed. From Table 5, the columnar structure is more likely to form in lower solute concentration, when the temperature gradient is at the same condition.

4.7 Continuous Grain Growth in ICP Spraying

In ICP, the flow rate of particles is slower (30-40 m/s) (Ref 27) than the other systems and thus gives the particles longer residence time in the plasma flame. During flight in ICP, the particles can be superheated more than melting point, and evaporation can even occur. When these droplets fall on the substrate, viscosity is very low to wet and to transform rapidly. However, the activation energy required to overcome nucleation is the sum of ΔG_i and ΔG_v, as shown in Eq 4 and 7. In the case of heterogeneous nucleation, nucleation can be greatly facilitated with lower activation energy on the condition that the previously solidified surface of deposit acts as seed. The magnitude of this effect is (Ref 47)

$$f(\theta) = \frac{(2 + \cos\theta)(1 - \cos\theta)^2}{4} \qquad \text{(Eq 15)}$$

where θ is the wetting angle between a growing nucleus and surface of the solid. Numerical values of $f(\theta)$ are listed in Ref 43. The activation energy for this case would be Eq 16, multiplying Eq 7 by Eq 15, that is:

$$\Delta G^0_{n,\text{heterogeneous nucleation}} = -\left(\frac{16\pi}{3}\right)\left(\frac{\sigma^3}{\Delta g^2}\right)\cdot f(\theta) \qquad \text{(Eq 16)}$$

A large decrease in θ can be expected from smaller activation energy ΔG^0_n. In the case of θ, which is zero—that is, liquid droplet is completely wetted on the previously deposited layer—the activation energy will become zero. Under this condition, the existing grains prefer growing continuously by itself to extra nucleating in the liquid. Thus, columnar grains can grow through the layers as far as the superheated liquid drops are supplied on it, as shown in Fig. 5-7. When the liquid drops are quenched somewhat rapidly, a dendrite grain can be developed. Figure 8 shows a YSZ particle collected at short distance from the spray nozzle to the water bath for rapid quenching with a dendrite microstructure on the surface.

Table 5 Minimum stabilizing temperature gradient for columnar grain growth of YSZ as a function of distribution coefficient for $D = 0.005$ mm^2/s, $V = 10^{-4}$ mm/s, and $m = -0.64$ K/wt%

k	$C_0 = 20$ wt.%	$C_0 = 10$ wt.%
0.1	0.023 K/mm	0.0115 K/mm
0.5	0.00256 K/mm	0.00128 K/mm
0.9	0.00028 K/mm	0.00014 K/mm

5. Conclusions

After melting, particles spheroidized by ICP almost kept their original chemical composition homogeneously from center to surface. XRD analysis and concentration measurements by EPMA confirmed that there was no selective vaporization or segregation at least during spraying. However, the average solute concentrations were different from particle to particle.

The layers deposited with particles of different solute concentrations showed a continuous concentration profile near their boundaries due to solute diffusion between layers. The solute rejection by diffusion occurred in a layer during solidification, but the interface condition of $(dT_q/dz)_{z=0} > m(dC/dz)_{z=0}$ led columnar grains to facilitate.

The degree of deformation of the droplet to splat was about 320%, and droplet thickness in the deposit varied between 2 and 3 μm, depending on the particle size.

An array of small pores existed on the splat boundaries. These pores may be the trapped gas from the plasma gas during spraying and affects microstructure by retarding the heat transfer.

The microstructure of the bottom part of the deposit showed equiaxed small grains. Equiaxed small grains were prevailed when the droplets were quenched rapidly on the substrate; this may be a large ΔT due to the rapid quenching. In the middle part of the deposit, large columnar grains, about 100 μm thick and 300 μm long, developed through the layers with strong adhesion between layers.

The magnitude of local thermal under cooling was estimated by 2.6 K. This small value may be due to the heat of droplets, latent heat of solidification, small pore array on the splat boundaries, as well as the low thermal conductivity, retarding heat transfer, and decreasing the solidification rate. Thus thick and long columnar grains could be facilitated.

For the columnar grains of a deposit of zirconia with 20 wt.% yttria by ICP, the minimum temperature gradient was inferred as a function of distribution coefficient by 0.023 to 0.00028 K/mm.

The long columnar grain growth through the layers was supposed to be possible, when the previously solidified surface of deposit acts as a seed.

Acknowledgments

The author would like to thank Dr. M.I. Boulos and Dr. F. Gitzhofer for providing invaluable assistance throughout the plasma spraying experiments in Canada and Professor S.S. Cho of Dept. of Metal. Eng. of Chungnam National University for reading and assistance with the manuscript. This project was carried out under the Nuclear R&D Program by Korean Ministry of Science and Technology.

References

1. W. Kurz, and R. Trivedi, Rapid Solidification Processing and Microstructure Formation, *Mater. Sci. Eng.*, 1994, Vol A179/180, pp 46-51
2. G.X. Wang, V. Prasad, and S. Sampath, An Integrated Model for Dendritic and Planar Interface Growth and Morphological Transition in Rapid Solidification, *Metall. Mater. Trans., A Phys. Metall. Mater. Sci.*, 2000, Vol 31A (No. 3), pp 735-746
3. G.X. Wang, S. Sampath, V. Prasad, and H. Herman, On the Stability of Rapid Planar Solidification During Melt-Substrate Quenching, *Mater. Sci. Eng.*, 1997, Vol A226-228, pp 1035-1038
4. M. Gaumann, R. Trivedi, and W. Kurz, Nucleation Ahead of the Advancing Interface in Directional Solidification, *Mater. Sci. Eng.*, 1997, Vol A226-22, pp 763-769
5. W. Kurz and D.J. Fisher, Solidification Microstructure-Cells and Dendrites *Fundamentals of Solidification*, Trans Tech Publications Ltd., Switzerland, 1998, p 82
6. J.D. Hunt, Steady State Columnar and Equiaxed Growth of Dendrites and Eutectic, *Mater. Sci. Eng.*, 1984, Vol 65, pp 75-83
7. I.H. Jung, K.K. Bae, M.S. Yang, and S.K. Ihm, A Study the Microstructure of YSZ Deposited by Inductively Coupled Plasma Spraying, *J. Therm. Spray Technol.,* 2000, Vol 9 (No. 4), pp 463-477
8. H. Katsushi, T. Masami, K. Hirokazu, and K.K. Kinoshita, Directional solidification of Inx Ga1− xAs, *J. Cryst. Growth,* 2000, Vol 21, pp 471-477
9. A. Ludwig and W. Kurz, Direct Observation of Solidification Microstructures Around Absolute Stability, *Acta Mater.*, 1996, Vol 44 (No. 9), pp 3643-3654
10. B. Drevet, H.N. Thi, D. Camel, B. Billia, and M.D. Dupouy, Solidification of Aluminium-Lithium Alloys Near the Cell/Dendrite Transition-Influence of Solutal Convection, *J. Cryst. Growth*, 2000, Vol 218, pp 419-433
11. M.C. Flemings, Plane Front Solidification of Single-Phase Alloys, *Solidification Processing*, McGraw-Hill, 1974, pp 32-44
12. W. Kurz and D.J. Fisher, Diffusion at a Dendrite Tip, *Fundamentals of Solidification*, Trans Tech Publications Ltd., Switzerland, 1998, p 240
13. W. Kurz, D.J. Fisher, Morphological Instability of a Solid/liquid Interface *Fundamentals of Solidification,* Trans Tech Publications Ltd., Switzerland, 1998, p 51
14. J.S. Reed, *Introduction to the Principles of Ceramic Processing*, John Wiley & Sons, 1988, p 17
15. W. Kurz and D.J. Fisher, Atom Transfer at the Solid/Liquid Interface, *Fundamentals of Solidification*, Trans Tech Publications Ltd., Switzerland, 1998, p 22
16. W. Kurz and D.J. Fisher, Atom Transfer at the Solid/Liquid Interface, *Fundamentals of Solidification*, Trans Tech Publications Ltd., Switzerland, 1998, p 29
17. E. Pfender, Thermal Plasma Thechnology: Where Do We Stand and Where Are We Going? *Plasma Chem. Plasma Pro*., 1999, Vol 19 (No. 1), pp 1-31
18. S. Sampath, X.Y. Jiang, J. Matejicek, A.C. Leger, and A. Vardelle, Substrate Temperature Effects on Splat Formation, Microstructure Development and Properties of Plasma Sprayed Coatings Part I: Case Study for Partially Stabilized Zirconia, *Mater. Sci. Eng.*, 1999, Vol A272, pp 181-188
19. S. Sampath, Microstructural Characteristics of Plasma Spray Consolidated Amorphous Powder, *Mater. Sci. Eng.*, 1993, Vol A167, pp 1-10
20. C. Moreau, P. Cielo, M. Lamontagne, S. Dallaire, J.C. Krapez, and M. Vardelle, Temperature Evolution of Plasma Sprayed Niobium Particles Impacting on a Substrate, *Surf. Coat. Technol.*, 1991, Vol 46, pp 173-187
21. L. Pawlowski, Coating Build-up, *The Science and Engineering of Thermal Spray Coatings*, John Wiley Sons, 1995, pp 122-127
22. C. Moreau, P. Cielo, and M. Lamontagne, Flattening and Solidification of Thermal Sprayed Particles, *Thermal Spray: International Advances in Coatings Technology,* C.C. Berndt, Ed., ASM International, 1992, pp 761-766
23. H. Bhat and H. Herman, Plasma Sprayed-Quenched Martensitic Stainless Steel Coatings, *Thin Solid Films*, 1982, Vol 95, pp 227-235
24. W. Kurz and D.J. Fisher, Atom Transfer at the Solid/liquid Interface,

Solidification, Trans Tech Publication, The Netherlands, 1984, pp 28-35

25. W. Kurz, D.J. Fisher, Introduction, *Fundamentals of Solidification*, Trans Tech Publications Ltd., Switzerland, 1998, p 16
26. V. Laxmanan, On Producing an Alloy of Uniform Composition During Rapid Solidification Processing, *ASM '86 International Conference: Processing of Structural Metals by Rapid Solidification* (Orlando, Florida, 6-9 October 1986), ASM International, 1986, pp 41-56
27. X. Fan, Induction Plasma Deposition of Alumina Free Standing Part, Ph.D. Thesis, University of Shebrook, Canada, 1994.
28. P. Scardi and Lutterotti, Microstructural Characterization of Plasma-Sprayed Zirconia Thermal Barrier Coatings by X-ray Diffraction Analysis, *Surf. Coat. Technol.*, 1993, Vol 61, pp 52-59
29. C.A. Anderson, J. Greggi, Jr., and T.K. Gupta, Diffusionless Transformation in Zirconia Alloys, *Science and Technology of Zirconia II, Vol. 12*, *Advanced in Ceramics*, N. Claussen, M. Ruhle, H. Heuer, Ed., The American Ceramic Society, 1983, p 80
30. S. Sampath and H. Herman, Microstructural Development of Plasma Sprayed Coatings, *12th International Thermal Spraying Conference* (London, U.K., 4-9 June, 1989), C. Coddet, Ed., ASM International, 1989, paper 53
31. R.W. Trice and K.T. Faber, Role of Lamellae Morphology on the Microstructural Development and Mechanical Properties of Small-Particle Plasma-Sprayed Alumina, *J. Am. Ceram. Soc.*, 2000, Vol 83 (No. 4), pp 889-896
32. S.H. Leigh and C.C. Berndt, Quantitative Evaluation of Void Distributions within a Plasma-Sprayed Ceramic, *J. Am. Ceram. Soc.*, 1999, Vol 82 (No. 1), pp 17–21
33. L. Pawlowski, Introduction, *The Science and Engineering of Thermal Spray Coatings*, John Wiley & Sons, 1995, p xv
34. R.H. Perry, and C.H. Chilton: in *Chemical Engineerings' Handbook, 5th ed*. McGraw-Hill, 1973, pp. 3-112.
35. E. Ryshkewitch and D.W. Richerson, *Oxide Ceramics Physical Chemistry and Technology*, *2nd ed*., Academic Press, 1985, p 378
36. K.K. Srivastava, R.V. Patil, C.B. Choudhary, K.V. Gokhale, and E.C. Subbarao, Reviced Phase Diagram of the System ZrO2-YO1.5, *Trans. J. Br. Ceram. Soc.*, 1974, Vol 73 (No. 3), pp 85-91
37. X.L. Jiang, Induction Plasma Spraying of Refractory Metals, Ph.D. Thesis, University of Shebrook, Canada, 1994
38. W.D. Kingery, H.K. Bowen, and D.R. Uhlmann, Microstructure of Ceramics, *Introduction to Ceramics*, *2nd ed*., John Wiley & Sons, 1976, p 449
39. Y.W. Kim, D.L. Bourell, and C. Persad, High Energy, High Rate Powder Processing of a Rapid Quenched Quaternary Alloy, Ni56.5Mo23.5Fe10B10, *Mater. Sci. Eng.*, 1990, Vol A123, pp 99-115
40. A.J.F. Craig and M. Hideaki, Molecular Dynamics Investigations of Grain Boundary Phenomena in Cubic Zirconia, *Comput. Mater. Sci.*, 1999, Vol 14, pp 177-184
41. T. Nakamura, G. Qian, and C.C. Berndt, Effects of Pores on Mechanical Properties of Plasma-Sprayed Ceramic Coatings, *J. Am. Ceram. Soc.*, 2000, Vol 83 (No. 3), pp 578-584
42. K.T. Faber, Microstructural Characterization of Small-Particle Plasma Spray Coatings, *J. Am. Ceram. Soc.*, 1999, Vol 82 (No. 8), pp 2204-2208
43. W. Kurz and D.J. Fisher, Solidification Microstructure-Cells and Dendrites, *Fundamentals of Solidification*, Trans Tech Publications Ltd., Switzerland, 1998, p 118
44. W. Kurz and D.J. Fisher, Solidification Microstructure-Cells and Dendrites, *Fundamentals of Solidification*, Trans Tech Publications Ltd., Switzerland, 1998, p 20
45. W. Kurz and D.J. Fisher, Solute and Heat Flux Calculation Related to Microstructure Formation, *Fundamentals of Solidification*, Trans Tech Publications Ltd., Switzerland, 1998, p 187
46. W. Kurz and D.J. Fisher, Solidification Microstructure-Cells and Dendrites, *Fundamentals of Solidification*, Trans Tech Publications Ltd., Switzerland, 1998, p 86
47. W. Kurz and D.J. Fisher, Atoms Transfer at the Solid/Liquid Interface, *Fundamentals of Solidification,* Trans Tech Publications Ltd., Switzerland, 1998, p 28